Supporting material:

Sunlight Induced Photo-thermal Synergistic Catalytic CO_2 Conversion via Localized Surface Plasmon Resonance of MoO_{3-x}

Jue Li,[a#] Yinghao Ye,[b#] Liqun Ye,[ad*] Fengyun Su,[a] Zhaoyu Ma,[a] Jindi Huang,[a] Haiquan Xie,[a] Dmitry E. Doronkin,[c] Anna Zimina,[c] Jan-Dierk Grunwaldt,[c] Ying Zhou,[b*]

a. Engineering Technology Research Center of Henan Province for Solar Catalysis, College of Chemistry and Pharmaceutical Engineering, Nanyang Normal University, Nanyang 473061, P. R. China.

b. State Key Laboratory of Oil and Gas Reservoir Geology and Exploitation, School of Materials Science and Engineering, Southwest Petroleum University, Chengdu, 610500, P. R. China.

c. Institute for Chemical Technology and Polymer Chemistry and Institute of Catalysis Research and Technology, Karlsruhe Institute of Technology, 76131 Karlsruhe, Germany.

d. College of Materials and Chemical Engineering, Key Laboratory of Inorganic Nonmetallic Crystalline and Energy Conversion Materials, China Three Gorges University, Yichang 443002, P. R. China.

Corresponding Author

* Prof. Liqun Ye

E-mail: yeliquny@163.com

* Prof. Ying Zhou

E-mail: yzhou@swpu.edu.cn

[#]The authors contributed equally.

Experimental section

1 Synthesis

1.1 Materials

Molybdenum metal powder, hydrogen peroxide (H_2O_2, 30 wt%), 1-butanol, and were respectively purchased from Macklin, Feng Chuan Technology Co., Ltd., DeNen Reagents Ltd., Kermel Reagents Ltd..

1.2 Synthesis of the plasmonic MoO_{3-x} nanosheets

In a typical synthetic procedure, 2 mmol of molybdenum metal powder was added to a beaker (50 mL) containing 24 mL of 1-butanol. Then 3 mL of H_2O_2 was introduced and magnetically stirred for about 30 min to obtain the transparent yellow solution. The solution was transferred to a PTFE reactor, sealed in a stainless steel autoclave, heated and maintained at 140 °C for 12 h. After cooling down to room temperature (no active cooling was used), the product was collected by centrifugation, rinsed with ethanol for three times and finally dried at 60 °C in a vacuum drying oven. The dried sample was ground and stored as MoO_{3-x}. For comparison, two more MoO_{3-x} samples were prepared using a similar procedure with ethanol and isopropanol as solvents.

1.3 Synthesis of the MoO_3 nanosheets

The prepared MoO_{3-x} sample was placed in a tube furnace and heated at 10 to 600 degrees per minute for 6 hours under an oxygen atmosphere. The calcined sample with oxygen vacancies filled during calcination was defined as MoO_3.

2 DFT Calculation

Density functional theory (DFT) calculations were performed using DMol3 procedure based on the Materials Studio software. The electron exchange and correlation were approximated by generalized gradient approximation (GGA) with the Perdew-Burke-Ernzerhof (PBE) functional. Dispersion correction by TS (DFT-D) was used to describe the van der Waals interaction. The valence electron configurations were $1s^1$ for H, $2s^22p^2$ for C, $2s^22p^4$ for O and $4d^54s^1$ for Mo, respectively. As for the Monkhorst-Pack grid k-point in the Brillouin-zone, a 5×5×1 k-point was used for geometry optimizations. For convergence threshold, the total

energy of the system, maxforce, and displacement tolerances were set to be 1×10-5Ha, 0.02 Ha/Å, and 0.05 Å, respectively. (J. Perdew, K. Burke, M. Ernzerhof, Generalized Gradient Approximation Made Simple, Physical Review Letters, 1996, 77, 3865-3868; Junli Zhang, Jiecai Fu, Fangyi Shi, Yong Peng, Mingsu Si, Luigi Cavallo, Zhen Cao, Hydrogen atom induced magnetic behaviors in two-dimensional materials: insight on origination in the model of α-MoO_3, Nanoscale, 2018, 10, 14100; Yue Peng, Wenzhe Si, Xiang Li, Jinming Luo, Junhua Li, John Crittenden, Jiming Hao, Comparison of MoO3 and WO3 on arsenic poisoning V_2O_5/TiO_2 catalyst: DRIFTS and DFT study, Applied Catalysis B: Environmental, 2016, 181, 692–698.)

3 Characterization

X-ray diffraction (XRD) analysis of the phases and crystal structures of the samples was conducted using a Bruker D8 diffractometer with Cu Ka radiation, and the scanning region was from 5° to 80° with the 2θ sweep speed of 6° min^{-1}. Morphology of the photocatalysts was imaged using a scanning electron microscope (SEM, ZEISS Sigma 500). The finer morphologies and lattices were studied by transmission electron microscope (TEM) JEM-2100F. UV-Vis diffuse reflectance spectroscopy (DRS) of samples were obtained by a UV-Vis spectrometer (HITACHI, UH4150) with a scanning range of 200-2100 nm. X-ray photoelectron spectroscopy (XPS) was performed on a Thermos Scientific ESCALAB 250XI X-ray photoelectron spectrometer (Al Ka, 150 W, and C1s 284.6 eV). Oxygen vacancies were identified by electron spin resonance (ESR) on a JES FA200 from JEOL. Photoluminescence spectra with the wavelength up to 1000 nm were acquired on a LabRAM HR Evolution Raman spectrometer (Horiba) with 785-nm laser excitation. A Quantachrome Autosorb-IQ automated gas sorption system was utilized to assess the Brunauer–Emmett–Teller (BET) surface areas at 77K. Time-resolved PL spectra (266 nm excitation) were recorded by a FLS980 Multifunction Steady State and Transient State Fluorescence Spectrometer (Edinburgh Instruments, room temperature). Transient absorption spectra were recorded at 260 nm by a NTAS Transient State absorption Spectrometer (Beijing Perfect light Technology Co., Ltd., China).

X-ray absorption spectra in terms of X-ray Absorption Near Edge Structure

(XANES) and Extended X-ray Absorption Fine Structure (EXAFS) were measured at the CAT end station of the CAT-ACT beamline at the Synchrotron Radiation Source at KIT, Karlsruhe.[A. Zimina, K. Dardenne, M. A. Denecke, D. E. Doronkin, E. Huttel, H. Lichtenberg, S. Mangold, T. Pruessmann, J. Rothe, Th. Spangenberg, R. Steininger, T. Vitova, H. Geckeis, J.-D. Grunwaldt, Rev. Sci. Instrum. 2017, 88, 113113.] The samples were measured ex situ at the Mo K absorption edge in transmission mode in form of pellets pressed with cellulose. The spectra were normalized, energy-corrected and the EXAFS background subtracted and Fourier-transformed (in the k-range 3 – 14 $Å^{-1}$) using the ATHENA program from the IFFEFIT software package.[B. Ravel, M. Newville, J. Synchrotron Radiat. 2005, 12, 537.]

4 Photocatalytic reduction of CO_2

The photocatalytic CO_2 reduction activity was measured in a Labsolar-III AG (Beijing Perfect light Technology Co., Ltd., China) closed gas system. After adding 5 ml of deionized water (provides the water vapor required for carbon dioxide reduction) to the reactor, a hollow perforated cylindrical support and a magnet were placed, and 0.05 g of the catalyst powder was evenly spread on the surface of the glass disc (28.26 cm^2). The glass disc is placed on the holder of the reactor. After the reactor was sealed under vacuum grease coating, the knob was turned on, purged with argon to remove air from the reactor, and then the knob was turned off. Subsequently, 1 ml of CO_2 was injected, and the gas was stirred with a magnet to obtain a uniform carbon dioxide atmosphere. After that, the reactor was irradiated from the top by a 300 W high pressure xenon lamp (PLS-SXE300, Beijing Perfect light Technology Co., Ltd., China). In the experiment, the whole spectrum is obtained by UV-visible infrared full-reverse reflective sheet, and the infrared-range light is obtained by adding a filter (> 800 nm), and the ultraviolet-visible is obtained by UV-visible full-reverse reflective sheet. The experiment with active cooling was performed at a constant temperature of 5 °C obtained using low-temperature thermostat bath (Shanghai Sunny Hengping Scientific Instrument Co., Ltd., China). During the irradiation, 1 mL of gas was taken from the reaction cell for subsequent qualitative analysis by GC9790II gas chromatography (GC, Zhejiang Fuli Analytical

Instrument Co., Ltd., China) equipped with a flame ionization detector (FID, GDX-01 columns). The quantification of the production yield was based on a calibration curve. The outlet gases were determined to be CO, CH_4 and CO_2.

5 Photoelectrochemical measurements

Transient photocurrent response and electrochemical impedance of the samples were measured in a three-electrode quartz cell containing Na_2SO_4 (0.5 M) electrolyte solution and using a CHI660E electrochemical workstation (CHI Instruments, Shanghai, China). Samples were located on a fluorinated-tin-oxide (FTO) conducting glass as the working electrode. Ag/AgCl and Pt played the role of reference and counter electrodes, respectively.

6 In-situ Fourier transform infrared spectroscopy (FT–IR) analysis

In-situ Fourier transform infrared spectroscopy was performed on a Nicolet IS–50 instrument. The sample was filled into an in-situ Harrick IR cell, and 1 atm CO_2 and H_2O vapors (room temperature) were introduced into the cell and fiber source (FX300, Beijing Perfect Light Technology Co., Ltd., Beijing, China) through the CaF_2 window of the cell. Before the measurement, the samples were degassed at 423 K for 4 h.

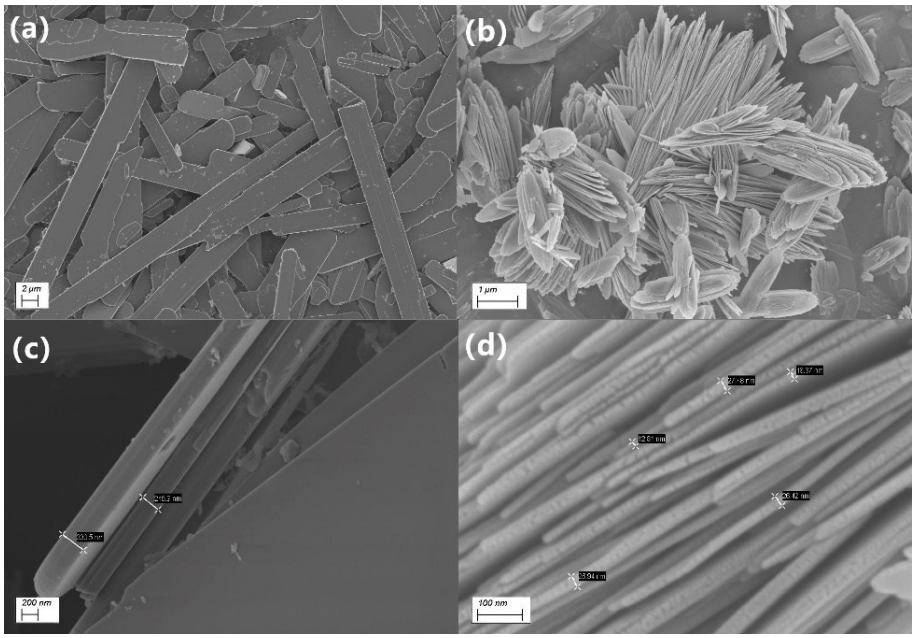

Figure S1 SEM of MoO_3 (a), (c) and MoO_{3-x} (b), (d).

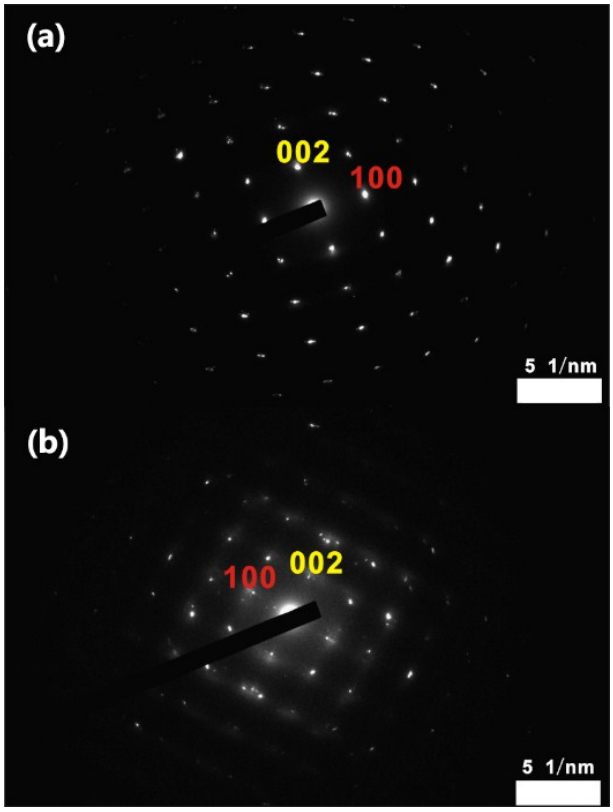

Figure S2 SAED of MoO_3 (a) and MoO_{3-x} (b).

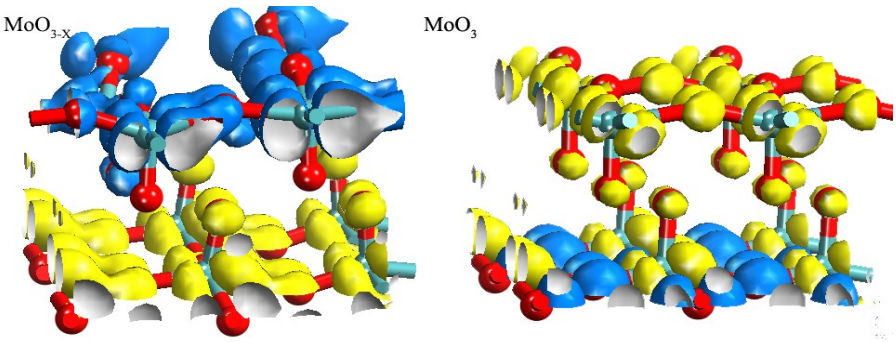

Figure S3 Highest occupied molecular orbital (HOMO) and lowest unoccupied molecular orbital (LUMO) of the MoO_{3-x} and MoO_3. The blue and yellow are HOMO and LUMO, respectively.

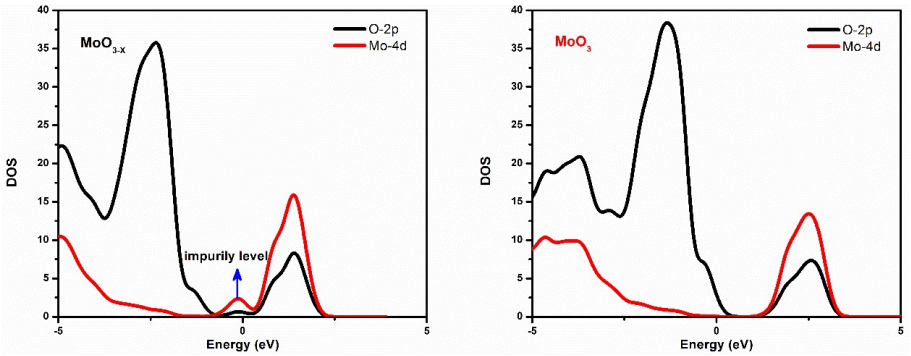

Figure S4 DOS of MoO_{3-x} and MoO_3.

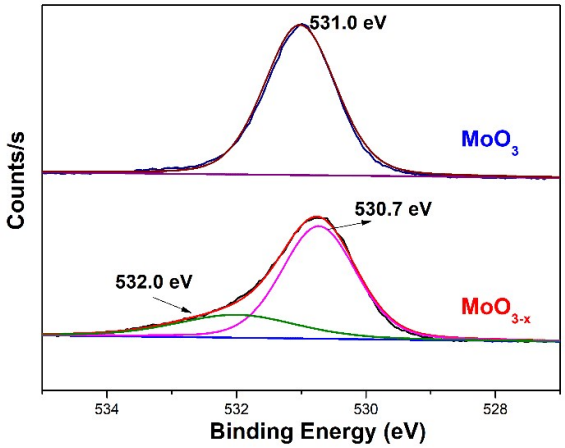

Figure S5 O1s XPS spectra of MoO_{3-x} and MoO_3.

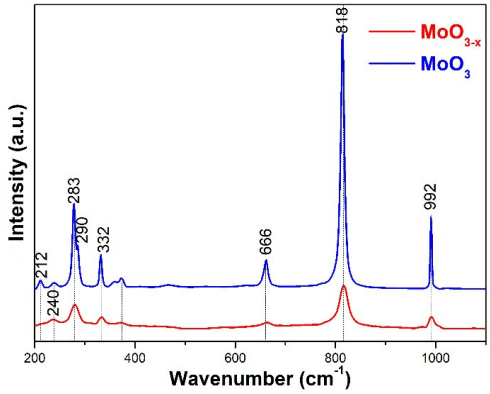

Figure S6 Raman spectrum of MoO_{3-X} and MoO_3.

Raman spectroscopy

The 283 cm^{-1} bond represents the bending mode for the double bond (Mo=O) vibration. The 666 cm^{-1} peak is assigned to the tri-coordinated oxygen (Mo_3–O) stretching mode, which results from edge-shared oxygen atoms in common to three adjacent octahedrons. The 818 cm^{-1} peak is related to the bi-coordinated oxygen (Mo_2–O) stretching mode, which results from corner-sharing oxygen atoms common to two octahedrons. The 992 cm^{-1} peak is assigned to the terminal oxygen (Mo=O) stretching mode, which results from an unshared oxygen. The peak at 332 cm^{-1} can be assigned to Mo_3–O and the two weak peaks at 212 and 240 cm^{-1} both represent the bending modes of Mo_2–O.[Nanoscale, 2016, 8, 8696-8703.] In the Raman spectra of MoO_{3-x}, compared with MoO_3, the peak intensity of MoO_{3-x} is significantly reduced. Some peaks are merging and even disappear, demonstrating the existence of oxygen vacancies in MoO_{3-x}.[Adv. Funct. Mater., 2016, 26, 91-100. ACS Appl. Mater. Interfaces, 2016, 8, 3482-3493.]

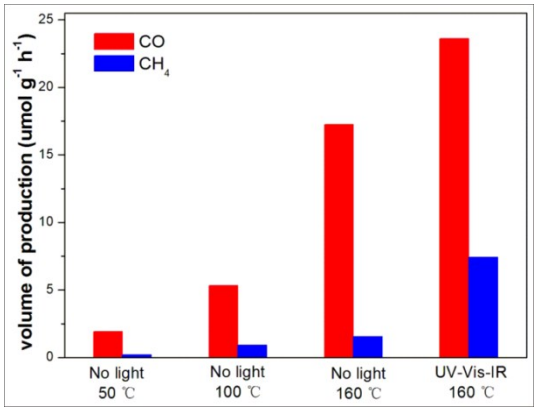

Figure S7 Thermal catalytic CO_2 reduction under different temperature without light irradiation.

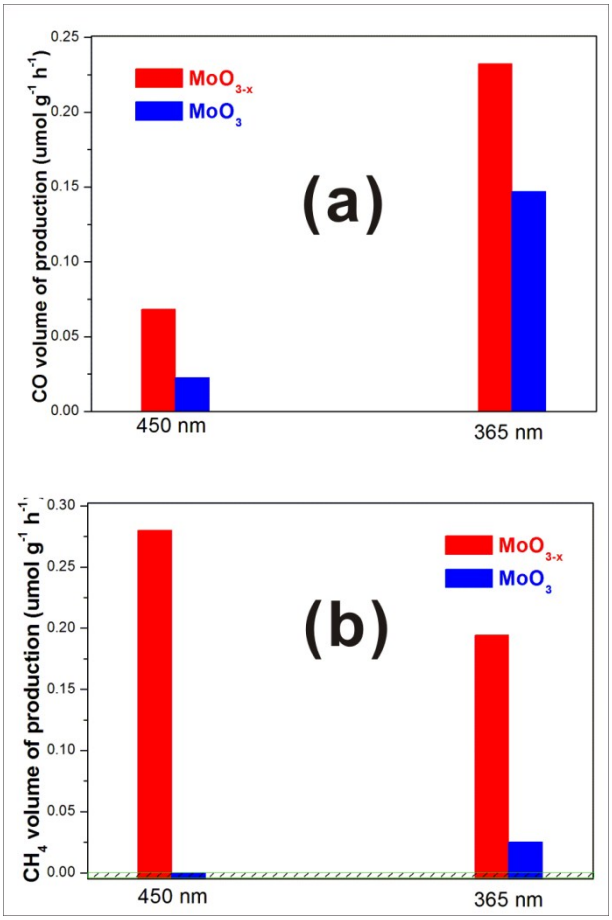

Figure S8 Photocatalytic CO_2 reduction under different wavelength LED light sources without heat effect.

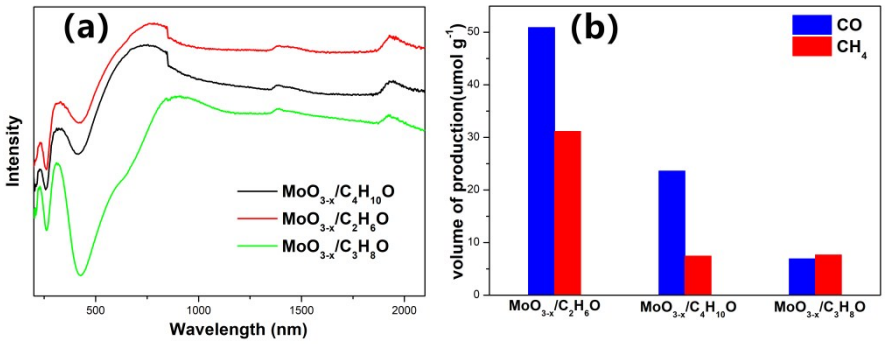

Figure S9 DRS spectrum and sunlight induced photo-thermal synergistic catalytic activity for CO_2 Conversion of MoO_{3-x} sample with ethanol, 1-butanol, isopropanol as solvent during MoO_{3-x} synthesis.

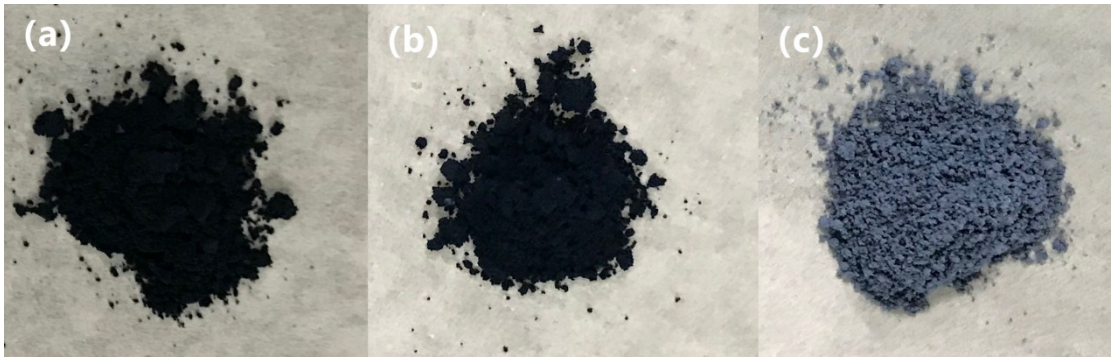

Figure S10 Photograph of MoO_{3-x} samples synthesized using (a) ethanol, (b) 1-butanol, (c) isopropanol as solvent.

Solvent used in preparation affects the concentration of oxygen vacancies. Here, ethanol, isopropanol and 1-butanol were used as solvents to prepare three MoO_{3-x} samples. As shown in **Figure S9**, based on the color and UV-Vis-IR absorption, the three MoO_{3-x} samples have different amount of the oxygen vacancies. And ethanol results in the highest number of oxygen vacancies. We compared the photocatalytic CO_2 reduction performance of three synthesized MoO_{3-x} samples. As shown in **Figure 10**, more oxygen vacancies result in the higher activity of MoO_{3-x}.

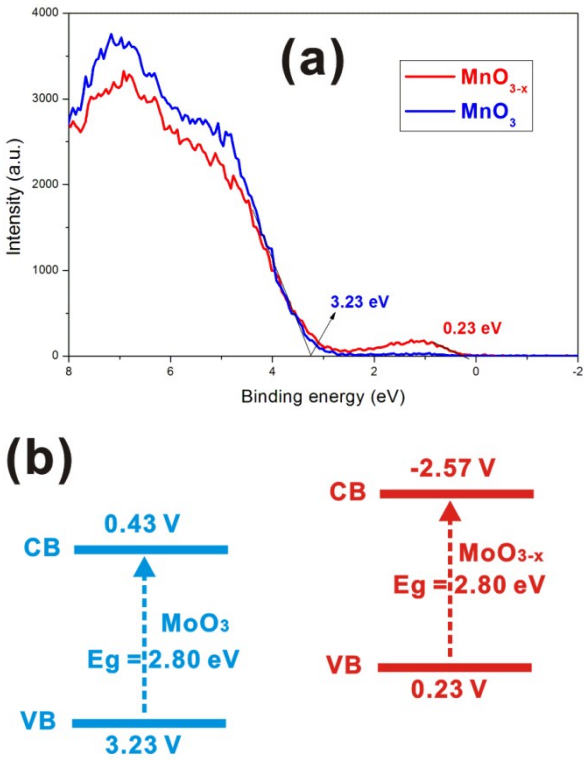

Figure S11 VB-XPS spectrum and band structure of MoO_3 and MoO_{3-x}.

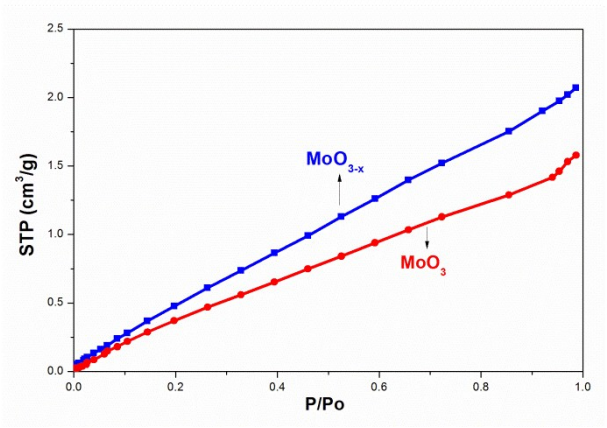

Figure S12 CO_2 adsorption of MoO_3 and MoO_{3-x}.

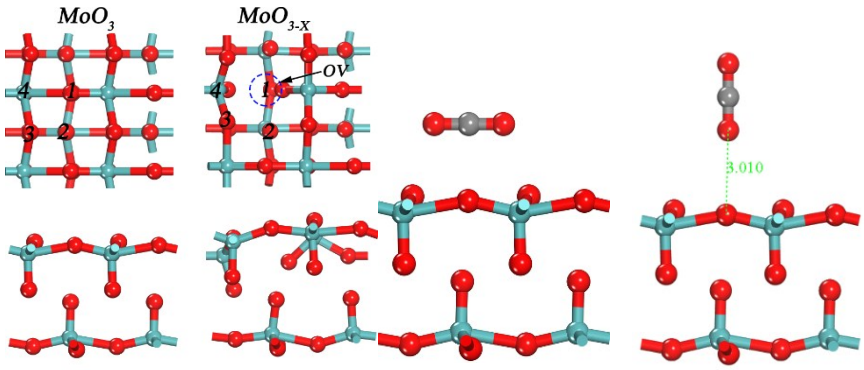

Figure S13 The configurations of CO_2 adsorption on the MoO_3 and MoO_{3-X} surface.

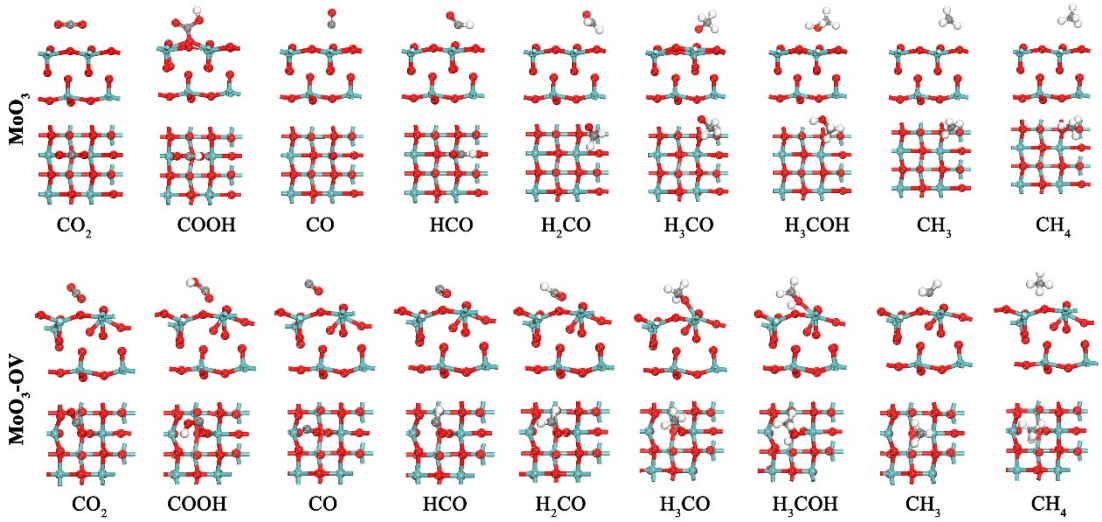

Figure S14 The structures of various CO_2 reduction products on MoO_3 and MoO_{3-x} surface.

Table S1 The energy of CO_2 adsorption on MoO_3 and MoO_{3-X} different sites

sites	MoO_3		MoO_{3-x}	
	Horizontal (eV)	Vertical (eV)	Horizontal (eV)	Vertical (eV)
1	-0.32	-0.10	-0.33	-0.38
2	-0.21	-0.08	-0.31	-0.07
3	-0.14	-0.08	-0.33	-0.08
4	-0.31	-0.17	-0.30	-0.30